Earth and Planetary Science
https://journals.nasspublishing.com/index.php/eps

RESEARCH ARTICLE

A Focus on Chemical Equilibria of Saline Aqueous Solutions Freezing under Ceres' Surface

Maria Pedone[1*], Edoardo Rognini[1], Eleonora Ammannito[1], Christina Plainaki[1], Maria Cristina De Sanctis[2], Andrea Raponi[2], Simone De Angelis[2], Mauro Ciarniello[2], Marco Ferrari[2], Alessandro Frigeri[2], Filippo Giacomo Carrozzo[2]

1. ASI, Agenzia Spaziale Italiana, 00133 Rome, Italy
2. IAPS, Istituto di Astrofisica e Planetologia Spaziali, INAF, 00133 Rome, Italy

Abstract: On Ceres' surface, the region including Kupalo and Juling was selected, in this study, for the geological aspects characterizing the area. Spectral data revealed that, at surface, the two craters show the presence of different carbonates: Na-carbonates (Kupalo) and Ca-Mg-carbonates (Juling). We think that the distinct geology at surface may be the result of the freezing of different subsurface aqueous reservoirs, characterized by different compositions and initial P-T conditions. The first step was to characterize the initial composition of aqueous solutions which, after freezing/precipitation processes, by using FREZCHEM code, delivered salts which can better approximate the surface compositions found by spectral analysis. Our potential brines were alkaline aqueous solutions, and they differ for the Na- and Cl- amounts (higher at Kupalo, rather than Juling solutions). The formation of hydrated sodium carbonate (natron, $Na_2CO_3 \cdot 10H_2O$) is highly favored in Na-enriched solution (e.g., Kupalo); instead, it could form only after water ice precipitation in Na-depleted solutions (e.g., in Juling). Natrite (Na_2CO_3) was found in Kupalo's surface layers, and, in our simulations, it did not directly precipitate from the solutions. We suggest that it could have been formed from natron and nahcolite ($Na_2CO_3 \cdot 10H_2O$ and $NaHCO_3$ respectively) at 1 bar of total pressure. Furthermore, we discussed the stability of the carbonates formed including $MgCO_3$ (magnesite) and $CaMg(CO_3)_2$ (dolomite). Finally, we investigated on the transport dynamics of brines suggesting that, already in the subsurface, there could be the physical processes to bring solid material (precipitated from the solutions) to the surface.

Keywords: Carbonates and salts-rich material; Ceres Dwarf Planet; Freezing processes; Brines

*Corresponding Author:
Maria Pedone,
ASI, Agenzia Spaziale Italiana, 00133 Rome, Italy
Email: maria.pedone@asi.it

Received: 20 June 2024; **Received in revised form:** 12 September 2024; **Accepted:** 29 September 2024; **Published:** 15 October 2024

Citation: Pedone, M., Rognini, E., Ammannito, E., et al., 2024. A Focus on Chemical Equilibria of Saline Aqueous Solutions Freezing under Ceres' Surface. *Earth and Planetary Science.* 3(2): 115–133. DOI: https://doi.org/10.36956/eps.v3i2.1139

DOI: https://doi.org/10.36956/eps.v3i2.1139

Copyright © 2024 by the author(s). Published by NanYang Academy of Sciences Pte. Ltd. This is an open access article under the Creative Commons Attribution-NonCommercial 4.0 International (CC BY-NC 4.0) License (https://creativecommons.org/licenses/by-nc/4.0/).

1. Introduction

The current state of knowledge concerning the characterization and evolution of Ceres, after the NASA *Dawn* mission was concluded is summarized in McCord et al.[1].

About surface composition, visible and infrared spectroscopic whole disk observations of Ceres using ground-based telescopes detected diagnostic electronic and molecular mineral absorptions[1]. The early observations and the reflectance spectra provided, during the NASA *Dawn* mission, from the Visible and InfraRed spectrometer (VIR[2]) revealed Ceres' surface is dark (albedo 0.09–0.1) and relatively uniform[3–6]. Ceres' reflectance spectra are consistent with minerals forming by aqueous alteration of chondritic materials[7–9], such as carbonates, and phyllosilicates[10–15]. The presence on Ceres' surface of Mg-phyllosilicates, NH_4-bearing species, and dark materials[15, 16] may suggest some aqueous alteration of the rocky body. At surface, abundant carbonates found[15, 16] can provide evidence of aqueous solutions at depth, and release toward the surface of the mineralogical associations found from *Dawn* mission.

Data from VIR revealed that different kinds of aqueous alteration occurred at the local scale, and some differences in carbonate compositions were detected[15]. For example, in Occator crater (whose formation was discussed by Scully et al.[17, 18]), the carbonate found, natrite (Na_2CO_3), is different from the Mg-Ca carbonate detected in the overall Ceres spectrum[19], and it was not observed in carbonaceous chondrites, generally considered as analogues of Ceres[9, 20]. Natrite is found in Enceladus' plumes[21], along with NaCl.

On Ceres, the origin of natrite was debated. The presence of natrite is related to relatively recent material that upwelled from the subsurface, such as occurred at Occator crater[9, 22]. Moreover, the presence of natrite was found in association with not-superimposed mounds and domes[15]. It was also detected in crater and rim ejecta, central peaks and floors, such as Kupalo and Haulani craters, or in bright spots, such as in Ikapati[15]. Some morphological settings, like floor fractures[23], may indicate that upwelling of salts-rich material may occur, induced by exogenous or endogenous causes, yet to be better determined (and not necessarily exclusive)[24].

According to Sizemore et al.[25] the formation of most morphologies is difficult to explain by impact processes only. The association of the domes with large impact structures is consistent with a cryovolcanic origin since the impact event may access deep layers of mobile material and/or produce melt pockets[26, 27].

To test the hypothesis of ascending brines in support of the subsurface aqueous origin of minerals found at the surface, we investigated the sequence and assemblage of solids precipitated during the freezing of potential initial reservoirs under a specific location on Ceres: the area of Kupalo and Juling craters. From a geological point of view, the target area is suitable to our investigation. In fact, these two geologically young craters host some of the brightest and most extensive Na-carbonates rich areas[15, 28]; and, in addition, from structural studies[29] the area was characterized by distinctive tectonics suggesting that probably endogenous processes modified both craters.

Such kind of geological features support a subsurface aqueous origin of hydrated Na-carbonates that are delivered to the surface from ascending fluids and their partial decomposition and dehydration on airless surface environments.

In this work, focusing on the freezing processes that may occur below the surface, we addressed specific problems that are summarized as follows:

- Can the mineralogical surface composition give any clues about the freezing processes themselves (e.g., in terms of different P-T conditions in which they have occurred)?
- Which are the solids to precipitate from brines (salty water bodies) frozen in the subsurface?
- What carbonates form during freezing?
- Where does natrite come from?

2. Saline aqueous solutions on ceres

Some results derived from data analysis[9] and some derived from modelling[30] suggested that, on Ceres, salts deposition, including ammonium salts (as NH_4Cl,[19]), and abundant natrite (Na_2CO_3), can form as

the consequence of ascending brines to the surface.

Within Occator crater, in which Na_2CO_3, NH_4Cl and $NaCl{\cdot}2H_2O$ [31] were found, Zolotov [30] showed that the initial solutions had a maximum temperature of 273 K, a maximum salinity of ~100 g per kg of H_2O, and a pH value of ~10.

Freezing models [30] and experiments [32] showed that, during decreasing temperature, solids (including water ice) precipitate from the initial aqueous solutions, increasing the ionic strength (in this work mentioned as *IS*). The solids that precipitate are water ice, hydrated forms of carbonates, sulphates, chlorides, that, like ammonium salts [33–35], are not stable at Ceres' surface conditions and dehydrate. Sulphates are not seen on Ceres [30] and may not be mentioned. Carbonates like $CaCO_3$, $MgCO_3$ and $CaMg(CO_3)_2$ can precipitate from freezing aqueous solutions, and association of Ca- and Mg- carbonates were found on the surface [15].

Precipitation of natron ($Na_2CO_3{\cdot}10H_2O$ [30]) can be followed by its dehydration [30] in such conditions, forming natrite (Na_2CO_3) which was detected on the surface [15, 19].

Bu et al. [36] reported quick dehydration of natron, occurring in a very short time of days to a few hundred years under Ceres' surface conditions, so that the deposition of hydrated Na-carbonate may be ongoing. Consequently, the brines exist within the dwarf planet today, and hydrated solids could be detected as has been done [31].

VIR spectral range and resolution did not allow to detect either gypsum or other sulphates on the surface. The potential lack of sulphates in Ceres' surface salts supports its similarity with bodies of the outer solar system [37].

Hydrohalite ($NaCl{\cdot}2H_2O$) has been detected recently in Occator crater [31] and chlorides were found along with sodium bicarbonate ($NaHCO_3$), and the ions that compose them are considered as possible constituents of Ceres' brines [31, 38].

In Occator, the original reservoir structure was debated [17, 38], as well as the possibility of upwelling of material from a zone placed between the "crust" and the "mantle" [39, 40]. The current model is that a partially crystallized briny reservoir can exist [41], and it contains salt-material with densities ≥2000 kg/m^3 mixed with low-density cryomagmatic constituents [38] such as clathrates and ice. By mixing high- and low-density material, the resulting brines could be characterized by densities (1140 kg/m^3, calculated by Quick et al. [38] below Occator) lower than the crust density (1300 kg/m^3 [40]) and, thus, could potentially ascend precipitating the solids that reached the surface.

Among upwelling scenarios, listed by Ruesch et al. [42, 43], a decompression of ascending gas-enriched ice has also been suggested [30, 42, 44–46].

In conclusion, there are several evidence on the presence of subsurface aqueous solutions that can ascend to the surface of Ceres dwarf planet.

3. Study area: Morphologies and main spectral features

Juling (coordinates: 36° S, 168.3° E, D=20 km) and Kupalo (coordinates: 39.6° S, 173° E, D=26 km) craters show well-defined rims and well-preserved ejecta, as shown in **Figure 1**, indicative of their young age [47, 48].

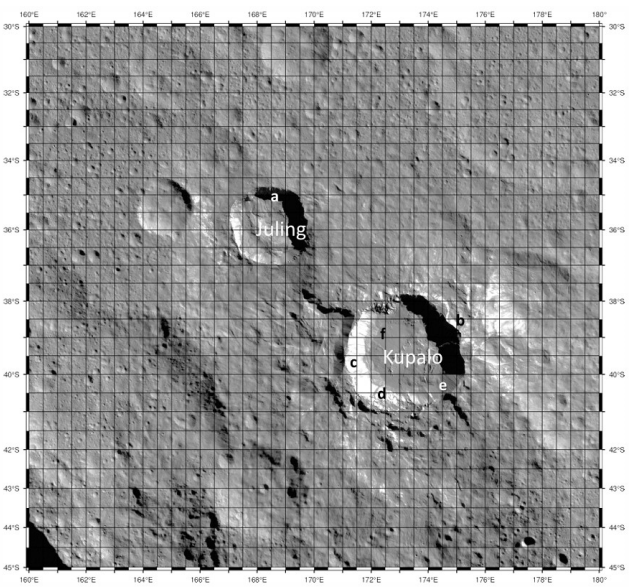

Figure 1. Context map of the study area with nomenclature and image mosaic (data from DLR). Juling crater is characterized by the northern shadowed water ice deposit (**a**) and by Ca- and Mg-carbonates (found throughout the area). At Kupalo, the presence of Na-carbonate (e.g., in **b–d**) is predominant, instead the presence of Ca- and Mg-carbonates (**e**,**f**) is very low.

By a morphological point of view, Kupalo crater displays well-preserved pitted materials, circumferen-

tial fractures, large floor fractures, channels, and a central ridge; instead, Juling is characterized by the presence of fractures (floor and circumferential), an interesting freshly resurfaced floor [49] without visible pits and peaks [25].

The two craters contain extensive bright predominantly carbonates-rich spots (rim and wall faculae [47]) and bright ejecta blankets. In Juling, the crater floor is not flat showing flows traces suggesting low viscosity material transport and the morphology revealed water ice presence [50, 51]. Ice signature was observed by VIR in the northern crater walls [51], and areas with carbonates are present [28]. High content of Na-carbonates is present in Kupalo crater (which correlates with the young age of Kupalo [48]), showing sharps rims that display a large amount of bright areas [28]. Spectral analysis of Juling and Kupalo [28] indicates some substantial differences in the chemical composition of carbonates: Juling, as well as most of Ceres, is rich in Ca-Mg carbonates, while Kupalo has mainly Na- carbonate [15, 19].

Supposing that morphological and spectral analysis on the surface may suggest some differences in the original compositions of brines frozen beneath the two craters, both solutions have probably suffered some physical-chemical differentiation leading to different kinds of carbonates on the surface.

4. Methods

4.1 Choice of the parameters and initial conditions to initialize our model

Pressure and temperature

FREZCHEM code was used to explore chemical processes in the Ceres' concentrated electrolyte solutions. In general, the code is initialized for concentrated electrolyte solutions and uses the Pitzer equations [52] to calculate the activity of water and the activity coefficients for soluble ions in the equilibrium between water and ice and between species in solution and solid phase salts.

Pitzer equations are used in temperature ranging from <-70 to 25 °C, pressure ranging from 1 to 1000 bar, and, moreover, it is applicable to a system composed by: Na-K-Mg-Ca-Fe-H-Cl-SO_4-NO_3-OH-HCO_3-CO_3-CO_2-CH_4-H_2O [53, 54].

The inputs of the code are molal concentrations of the main ions (e.g., Na^+, Cl^-, $SO_4{}^{2-}$...), alkalinity, pH, pressure, initial and final temperature, and step of decreasing temperature; while the outputs are final concentrations, activities, and moles of ions remaining in the solution phase. In addition, in the output, the solid phase species (ion-pairs) are also grouped including the moles and the equilibrium constant (k_{sp} in the following sections) for the reaction [53] at given P-T conditions.

Moreover, using FREZCHEM it is possible to simulate the freezing process under two pathways: equilibrium vs. fractional. Under equilibrium crystallization, solid phases that have precipitated are allowed to dissolve again and precipitate as different minerals. Under fractional crystallization (this case), a precipitated solid phase is not allowed to subsequently dissolve or re-precipitate.

Moreover, the choice of pressure and temperature parameters was crucial. The initial values of total pressure of 1, 1.5 and 30 bar were selected, in our work, in the attempts to find some differences (if there are any) during the freezing processes of brines in the subsurface, in the corresponding depths of 300 m, 500 m, and 10 km, at initial brines' densities ($\sim$1100 kg/m^3, calculated by FREZCHEM), and at gravity acceleration (g) of 0.28 m/s^2.

In our simulations, decreasing temperatures from 273 to 245 K were selected, and they are relevant since 273 K (liquid temperature) is the melting point of pure ice and 245 K (solid temperature) is the eutectic temperature for the Ceres' crust composition [55]. These are the temperatures of the brines, not the temperatures of the hosting rocks. Considering the thermal gradient of 2 K/km, given by Castillo-Rogez et al. [55], the temperatures at the surface should be of 150 K. Some authors [56] found that temperature at surface associated with some bright spots can be higher. Warmer surface areas (T=235±4 K) were also found by Saint-Pe, Combes and Rigaut [57]. A higher value of daily temperature (up to $\sim$240 K) was also found by modeling ice-rich area on Ceres, with ice buried 2 cm beneath the surface [35]. These higher temperature values are consistent with maximum daytime temperature value found on Ceres by VIR using its spectral range between 4.5 μm and 5.1

μm, where thermal emission dominates the acquired signal [58]. In this work, we also simulated the surface temperature of the two target craters (**Figures 2** and **3**), by applying an evolution of thermophysical model [59, 60]. The model provides temperature as a function of thermal conductivity and roughness, and, here, for the first time and in a testing mode, we added the information about the grainsize ranged 1–100 μm associated, respectively, to "dry material" [61] and water ice [51].

In the phase equilibria analysed by Zolotov [30] the temperature of brines was selected in a range of 298–245 K (at P=1 bar). The author reported that the formation of water ice occurs at T=269–273K. For lower temperature values, after water ice, the formation of all other solids may proceed [30].

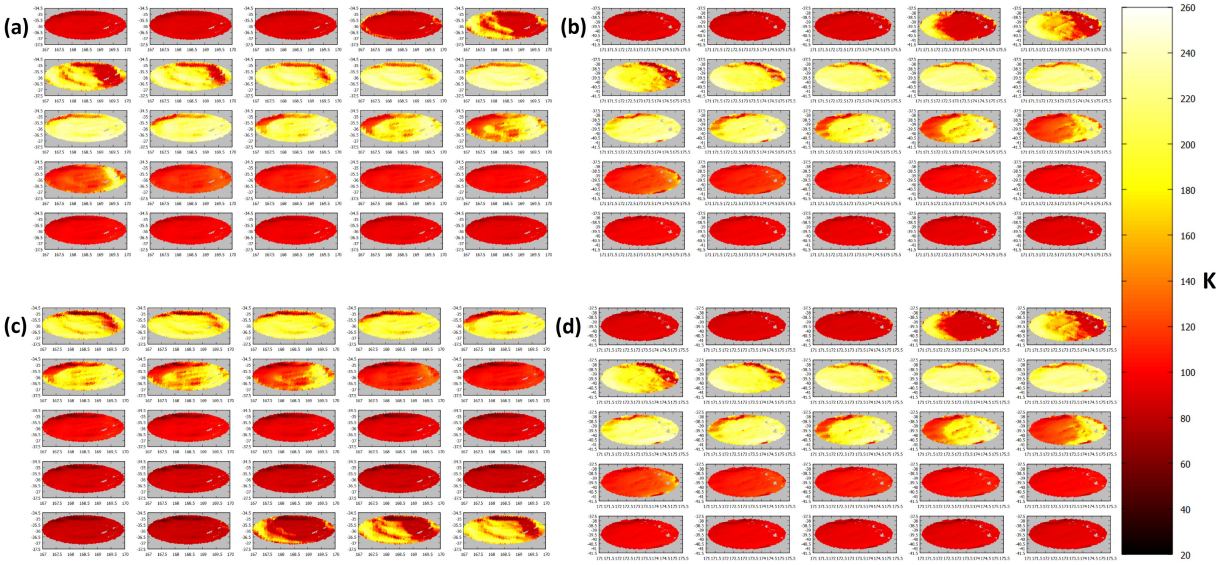

Figure 2. Surface temperatures derived by the thermophysical model [59, 60] modified by adding grainsize (1 μm) to the model. In detail: **a**) Juling perihelion; **b**) Kupalo perihelion; **c**) Juling aphelion; **d**) Kupalo aphelion.

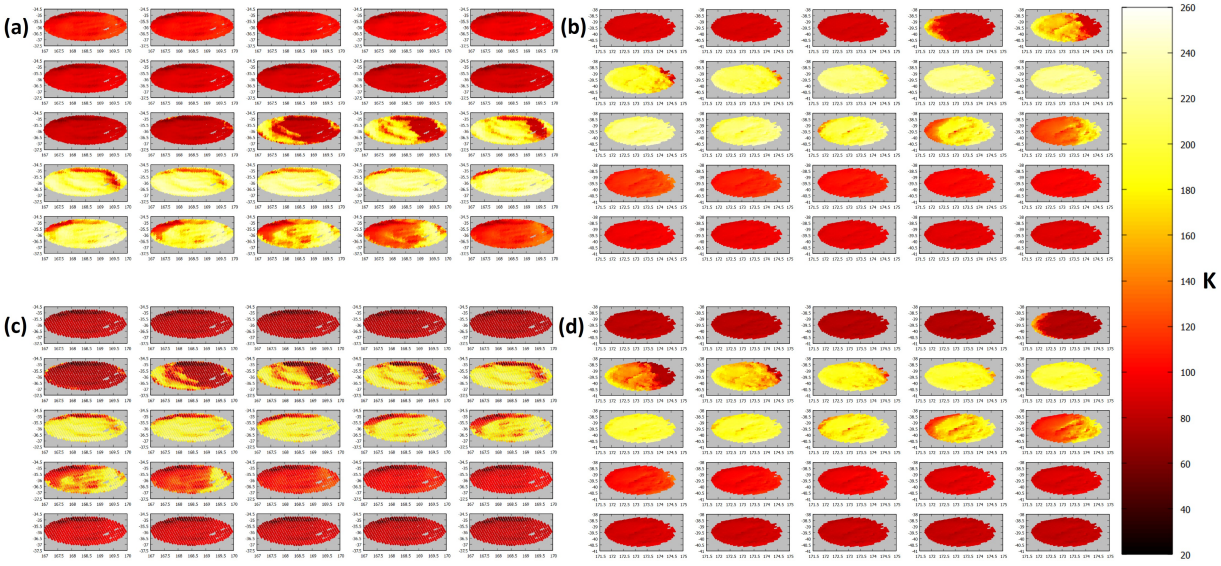

Figure 3. Surface temperatures derived by the thermophysical model [59, 60] modified by adding grainsize (100 μm) to the model. In detail: **a**) Juling perihelion; **b**) Kupalo perihelion; **c**) Juling aphelion; **d**) Kupalo aphelion.

Composition of initial aqueous solutions

The formation of salt deposits also depends on brines' composition that allow different kind of bright spots to form in some regions of Ceres [47].

In the attempt to characterize the initial aqueous solutions of Kupalo and Juling, we started from the work of Zolotov [30] that focused on bright salt deposits in Occator crater, rich in Na- carbonate [9, 19]. Starting from a reservoir with maximum temperature of 273 K, a salinity of 100 g per kg of H_2O, and characterized by pH∼10, Zolotov's [30] freezing models revealed early formation of natron ($Na_2CO_3 \cdot 10H_2O$) followed by a minor amount of nahcolite ($NaHCO_3$). The author concluded that Occator's deposits formed following the sublimation of ice after surface exposure and by airborn deposition of salty ice grains from plumes. Then, the dehydration of natron and nahcolite to form natrite occurred.

In this work, we first initialized the model inferring initial elemental composition of aqueous solutions under Kupalo and Juling (**Table 1**) under physical conditions as in Zolotov [30].

Abundances of the main cations and anions are shown in **Table 1**.

Chlorine (Cl^-) and inorganic carbonated species (CO_3^{2-} and HCO_3^-) are the main anions, expressed in mol/kg, deriving from the dissolved solids in the aqueous solution (chlorides and carbonates, respectively). Among inorganic C-species, dissolved CO_2 is a minor component in alkaline solutions [30] and here we consider an initial CO_2 content of about $1.3–1.5 \cdot 10^{-5}$ mol/kg in line with the literature (**Table 1**). Very low amount of CO_2 as gas phase ($CO_{2,(g)}$) cannot be excluded. The discussion about the effect of gas is addressed further.

The alkalinity value (Alk, **Table 1**) is the total amount of CO_3^{2-} and HCO_3^- expressed in equivalents/kg of water [62] obtained by the concentrations (in mol/kg) multiplied for the charge number ($2CO_3^{2-}+HCO_3^-$). This value of about 1.20 equivalents/kg was used to initialize the model (input of FREZCHEM). Moreover, VIR spectral features cannot confirm nor rule out the presence of sulphates on the surface of Ceres. We explored, as hypothesis of our study, that dissolved sulphates (SO_4^{2-}) could be present in solutions (in maximum concentration of 0.1 mol/kg) or not (0 mol/kg) as shown in **Table 1**. Finally, OH^- values are consistent with pH of solutions.

About the cations, for Kupalo, we suggest that it is mostly characterized by sodium carbonates at surface respect to the Ca- and Mg-carbonates. Initial sodium concentration was 1.8 mol/kg at Kupalo, higher than the concentrations of Ca^{2+} and Mg^{2+} ions.

The initial chemical compositions of Kupalo and Juling solutions are compared with Occator solutions (A, B, C given in Zolotov [30]; see **Table 1**). In **Table 1**, "Occator A" is the average composition, "Occator B" refers to the maximum reported abundance of Na_2CO_3 and "Occator C" represents the minimum abundance of Na_2CO_3.

Table 1. The initial composition of aqueous solutions in this work (Kupalo and Juling) compared to Occator's data (A, B, C; given in Zolotov [30].

Crater	Cl^-	OH^-	CO_2	$CO_{2,(g)}$	HCO_3^-	CO_3^{2-}	SO_4^{2-}	NH_3	Na^+	Ca^{2+}	Mg^{2+}	Alk	X	Y
Kupalo	0.1	$2.50 \cdot 10^{-4}$	$1.38 \cdot 10^{-5}$	$3 \cdot 10^{-4}$	$7.05 \cdot 10^{-2}$	0.56	0–0.1	0.055	1.8	$5 \cdot 10^{-6}$	$3.16 \cdot 10^{-5}$	1.19	42.81	40.88
Juling	0.04	$3.00 \cdot 10^{-5}$	$1.57 \cdot 10^{-5}$	$3 \cdot 10^{-4}$	$5.11 \cdot 10^{-2}$	0.60	0–0.1		0.2	$5.4 \cdot 10^{-6}$	$2.4 \cdot 10^{-5}$	1.25	44.97	17.38
Occator A	0.04	$7.74 \cdot 10^{-5}$	$8.74 \cdot 10^{-6}$		$1.63 \cdot 10^{-1}$	0.79		0.045	1.6			1.74		
Occator B	0.01	$2.31 \cdot 10^{-4}$	$1.16 \cdot 10^{-6}$		$6.43 \cdot 10^{-2}$	0.88		0.026	1.8			1.82		
Occator C	0.08	$3.34 \cdot 10^{-5}$	$3.63 \cdot 10^{-5}$		$2.90 \cdot 10^{-1}$	0.67		0.055	1.4			1.63		

Note. The dissolved species are expressed in molal concentrations (i.e., moles/kg of water), except for Ca and Mg (expressed in moles). NH_3 dissolved values suggested by literature [30] are also in mol/kg.
Low amount of CO_2 in gas phase ($CO_{2,(g)}$) is reported in line with P-T model and expressed in bar. Alkalinity values (Alk) are expressed in equivalents/kg of water (see text).
Finally, X and Y values, in the last two columns, were used to plot the aqueous solutions as in the Langelier-Ludwig diagram [63] in **Figure 4**.

In **Table 1**, X and Y values (two last columns) were used to plot the given solutions as in the Langelier-Ludwig diagram [63].

X and Y values were calculated starting from the amounts of the main ions (mol/kg) and alkalinity (equivalents/kg) as follows:

$$X = \frac{50\,(Alk)}{Alk + Cl^- + SO_4^{2-}} \quad (1)$$

$$Y = \frac{50\left(Na^{+}\right)}{Na^{+} + Ca^{2+} + Mg^{2+}} \quad (2)$$

From a compositional point of view, the solutions in the Kupalo and Juling reservoirs were characterized by the predominance of carbonated species (HCO_3^- + CO_3^{2-}), but they differ for the alkaline/alkaline-earth contents, falling into two different quadrants (**Figure 4**).

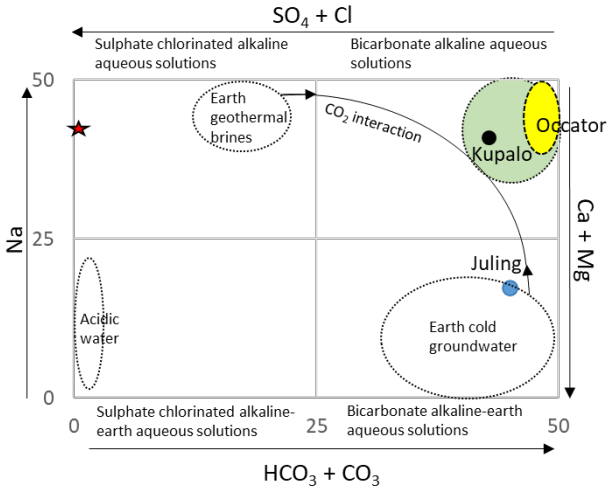

Figure 4. Langelier-Ludwig diagram [62] showing Ceres' brines in comparison with the main aqueous targets on Earth. To give one (of many) example of the Langelier-Ludwig diagram and the terrestrial targets see Minissale et al. [64]. The fields of the acidic water, geothermal brines, and cold groundwater are given. Occator solutions' (black dashed) and Kupalo solutions fall into the field of sodium bicarbonate waters on Earth. Earth seawater, characterized by conservative behaviour of the main ions, is plotted as a unique point (red star).
Kupalo (black coloured) and Juling (blue coloured) solutions are given at total pressure values from 1 to 30 bar (this study).

Since the diagram considers the aqueous solutions from a chemical point of view (anions/cations contents) excluding physical properties, we may explore the possibility to see our given solutions in a broader perspective making analogies and comparison with terrestrial solutions. If they were natural waters on Earth, they would be like bicarbonate-solutions with different metals contents falling in between main terrestrial endmembers (**Figure 4**).

We assume that Juling solutions are more like the Earth cold groundwater field [63] (**Figure 4**). Juling composition, in terms of the type of carbonate, is more like the Ceres average material [19] that is characterized by the presence of Ca-Mg carbonate and absence of natrite or hydrated Na carbonate [15], thus we can assume that also Ceres average material can be in the same quadrant of Juling solutions.

Instead, Kupalo solutions are assumed to be a mixture of Earth geothermal brines and cold groundwater-like (**Figure 4**). Kupalo (like Occator solutions' field; black dashed in **Figure 4**) falls in the field of sodium bicarbonate waters on Earth (green coloured circle in **Figure 4**).

Finally, it should be noted that Occator bright material has different mineralogy with respect to Ceres average composition and, in the diagram, it is in a different quadrant with respect to the one characterizing Juling (and Juling-like) compositions.

Decreasing temperature step

In our simulations, 5K of decreasing temperature step, between the initial and the final T value, was selected. The 5K and 1K modelling steps have given similar results in terms of T-range in which each solid precipitated from the solution, and in terms of order of precipitation of solids during the freezing. Here, we give an example of output by using 1 K decreasing model for Kupalo solutions at 1 bar (**Figure 5**). As shown in **Figure 5**, at T=273 K $CaCO_3$, $MgCO_3$ and $CaMg(CO_3)_2$ precipitated from the solution, and, at T=270 K water ice formation occurred. At 252<T<270 K, the precipitation of $MgCO_3$, $CaMg(CO_3)_2$, $Na_2CO_3 \cdot 10H_2O$ and water ice occurred, and their concentrations decreased except for two peaks of concentrations at T=257 K and T=268 K. This anomalous trend could be due to the starting formation of such kinds of sulphates reported by the simulation (not shown in **Figure 5**). Finally, close to the eutectic temperature (T=248 K) $NaHCO_3$ precipitated. The code stopped to run at the precipitation of hydrohalite ($NaCl \cdot 2H_2O$) occurred at T=248 K, but it was not possible to quantify its moles number (like in the 5K step model).

Therefore, for all the cases we used the 5K T-step, which was a good compromise to find differences (if any) in the freezing processes beneath the two craters, and we achieved results which, as shown as follows, where comparable, turned out in line with the findings of other authors.

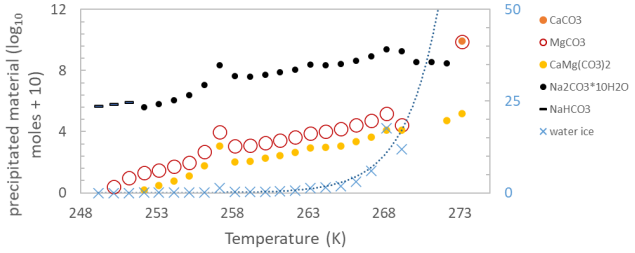

Figure 5. Example of results deriving from the freezing simulations applied to aqueous solutions under Kupalo crater at 1 bar (1 K decreasing model). The amounts of the solids precipitated (left y-axis), expressed in log10 moles + 10, were calculated starting from the initial water content of 1000 g at Ti=273 K decreasing to 0.1 g at the eutectic final temperature. Water ice amounts, expressed in moles, are plotted in the right y-axis (in blue). Water ice is characterized by an exponential decrement (dotted blue curve) during the freezing simulations. Here only carbonates, water ice and sodium bicarbonate were shown.

4.2 Summary of initial conditions

Summarizing, freezing processes that occurred in our initial aqueous solutions given in table 1 were simulated by using FREZCHEM fractional crystallization pathway by changing temperature value from the initial T_i=273 K to final T_f=243 K, and at decrement step value of ΔT=5 K.

Pressure values of 1, 1.5 and 30 bar were considered in our models, which correspond to a depth value from 300 m to 10 km (at initial density of about 1000 kg/m^3 at 273 K, and at g=0.28 m/s^2).

The code calculated the amounts of solid phases (salts and water ice expressed in moles) that precipitated, from the initial solutions, during each step of decreasing temperature.

The pH value of the given solutions is ∼10 as suggested from Zolotov[30], and the alkalinity is ∼1.2 equivalents/kg of water.

The results of our model are presented in the following section.

5. Results

5.1 Solids precipitation from initial aqueous solutions

Figures 6 and **7** show the results derived from the freezing simulations applied to aqueous solutions in Kupalo and Juling craters, respectively, at three different pressure conditions (1, 1.5 and 30 bar).

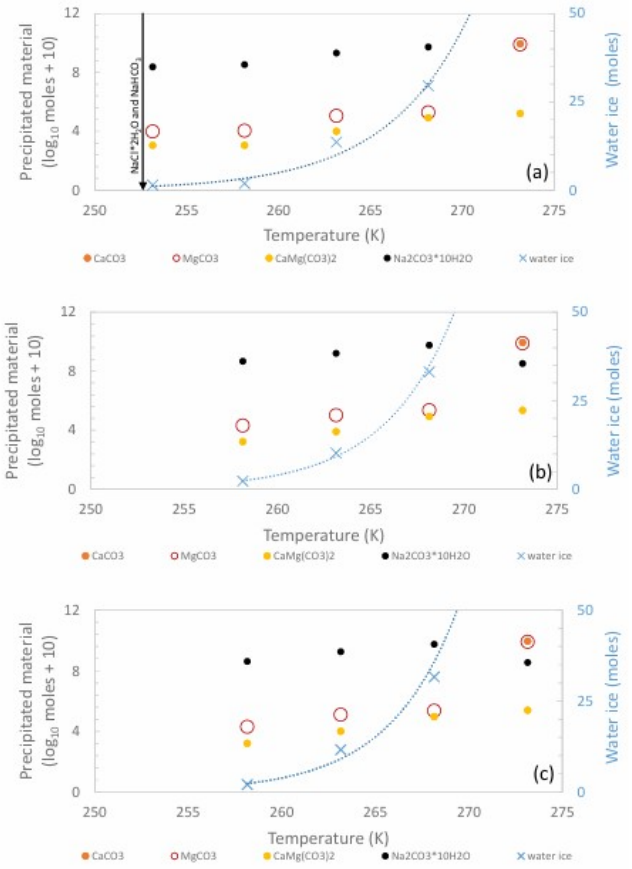

Figure 6. Results deriving from the fractional freezing simulations applied to aqueous solutions under Kupalo crater at three different pressure conditions: (**a**) 1 bar, (**b**) 1.5 bar, and (**c**) 30 bar. The amounts of the solids precipitated (left y-axis), expressed in log10 moles + 10, were calculated at each ΔT step starting from the initial water content of 1000 g at Ti=273 K decreasing to 0.1 g at the eutectic final temperature. Water ice amounts, up to 50 moles, are plotted in the right y-axis (in blue). The precipitation of sulphates and chlorides is discussed in the text.

In detail, the amounts of the solids, expressed in moles (up to 1 except for water ice), were calculated starting from the initial water content of 1000 g at T_i=273 K decreasing to 0.1 g at the eutectic final temperature, that here was >250 K (in both cases the code stopped before the simulations arrive at the chosen T_f value).

In **Figures 6** and **7**, the main vertical axis is referred to a log scale ($\log_{10}$ moles + an offset) of the amounts of precipitated solids (except for water ice) formed at each ΔT step. Water ice amounts, up to 50 moles, were plotted in the secondary vertical axis (blue coloured in **Figures**

6 and **7**).

A first consideration is that, as the temperature decreases, there is the precipitation of minerals/salts. The formation of water ice occurred at T=268 K (in line with results given by Zolotov[30] that reported the ice formation at T<270 ± 2 K), and its production exponentially decreased for lower temperature (blue dotted curves in **Figures 6** and **7**). All the values found reflect the 5 K step of decreasing temperature.

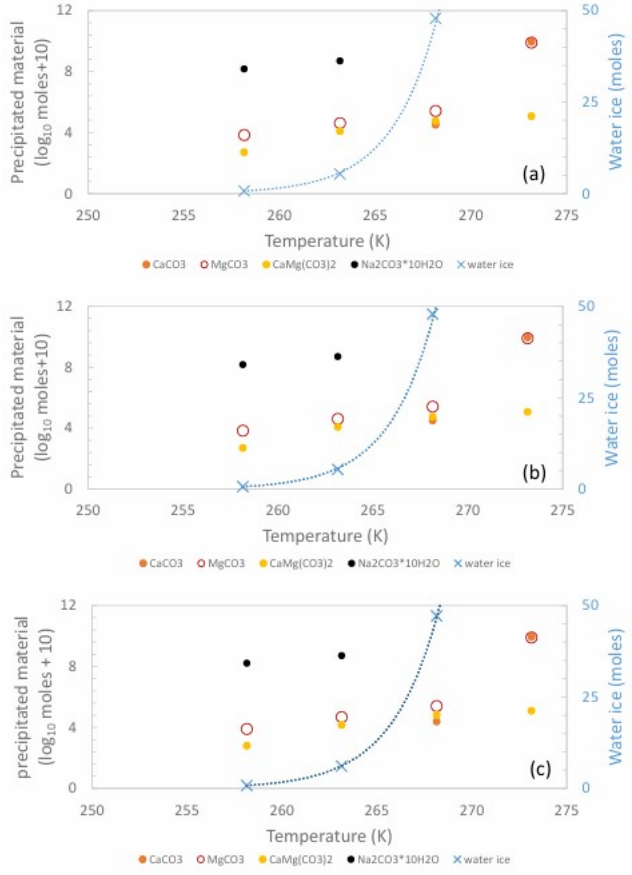

Figure 7. Results deriving from the fractional freezing simulations applied to aqueous solutions under Juling crater at three different pressure conditions: (**a**) 1 bar, (**b**) 1.5 bar, and (**c**) 30 bar. The amounts of the solids were indeed and shown as expressed in **Figure 6**.

During the simulations, $MgCO_3$, $CaCO_3$ and $CaMg(CO_3)_2$ were the first solids to precipitate from solutions (before water ice formation) at the first ΔT step at 1, 1.5 and 30 bar (**Figures 6** and **7**). As regards hydrated sodium carbonate (black dots in **Figures 6** and **7**), in Kupalo, natron ($Na_2CO_3 \cdot 10H_2O$) can form simultaneously (**Figure 6a**) or before (**Figure 6b,c**) water ice formation. Instead, in Juling, natron can precipitate only after water ice formation (**Figure 7a–c**).

This suggests that the formation of hydrated sodium carbonate was favored in sodium-enriched solutions (e.g., in Kupalo). Instead, calcium and magnesium carbonates are favored in both solutions at relatively higher temperatures.

If there were dissolved sulphates in brines, $Na_2SO_4 \cdot 10H_2O$ can form at T=268 K (not shown in **Figures 6** and **7**).

However, VIR spectral range and resolution did not allow to detect either gypsum or other sulphates on the surface, and, for this reason we don't discuss further their precipitation and stability. We just noted that sulphates and chlorides can precipitate from freezing aqueous solutions after carbonates. Moreover, by running the code with SO_4=0 mol/kg, the output concerning the precipitation of carbonates does not change.

In all cases, when the simulation stopped at eutectic (at 248<T<253 K, **Figure 6a**; or T<258 K, **Figures 6b**,**c** and **7a–c**), liquid water content was <0.1 g and no more calculations could be made by the code. Only in a case, in the last ΔT step (**Figure 6a**) and exactly at T≤251 K (**Figure 5**), for Kupalo, at 1 bar of total pressure, FREZCHEM returned a message invoking that $NaHCO_3$(nahcolite, $5–8 \cdot 10^{-5}$ mol) precipitated (black arrow in **Figure 6a**, black dash symbols in **Figure 5**). Moreover, at eutectic, $NaCl \cdot 2H_2O$ (hydrohalite, black arrow in **Figure 6a**) also precipitated, but neither 1K nor 5K step model was able to quantify the moles number of that solid.

Our results indicated that: 1) some solutions (Kupalo at 1 bar, **Figure 6a**) can exist, partially unfrozen, for T=255 K; and 2) in sodium enriched solutions (for which the code ran for T<255 K; **Figure 6a**) sodium salts appeared in the late stage of freezing processes occurring at shallower depths. Hydrohalite and nahcolite did not form in simulations carried out for pressure >1 bar, and they never appeared in freezing models of Juling solutions.

5.2 Solids-solutes equilibria calculations

During the freezing processes, decreasing water amounts affect the ionic strength (*IS*) of solutions.

The ionic strength of solutions (*IS*, expressed in

mol/kg; Equation (1)) has the formula as follows:

$$IS = \frac{1}{2}\sum_{i=1}^{N} \gamma c_i z_i^2 \quad (3)$$

where the activity coefficient (γ) multiplied for concentration values (c_i) allow to calculate the activities of positive and negative *i*-ions, and where z_i^2 is the charge square of *i*-ions.

Ionic strengths of solutions under Kupalo and Juling, are expressed in mol/kg and derived from the code. As shown in **Figure 8**, *IS* values increase as aqueous solutions are frozen.

The code returns as output the parameter k_{sp}. The quantity k_{sp} is defined as a "solubility product" that is the product of the solutes' activities, at equilibrium, in which a solid dissociates in solutes,

$$k_{sp} = [a_i]_{eq}^{n} \cdot [a_j]_{eq}^{m} \quad (4)$$

where *a* is the activity for each (*i-j*)-dissolved ions, *n* and *m* are stoichiometric parameters.

The k_{sp}value is the equilibrium constant. It appears in the formula of the Gibbs free energy values (ΔG> 0, ranged from 3.4·103 to 7.9·104 J·mol^{-1}, **Figure 8a,b**) as follows:

$$\Delta G = -\left[log\left(k_{sp}\right)\left(2.303\right)\left(R\right)\left(T\right)\right] \quad (5)$$

where T is temperature expressed in Kelvin at 5 K intervals, and R is a universal constant (R=8.3 J·K^{-1}·mol^{-1}).

The k_{sp} parameter (given from the code) has the same formula of IAP (Ionic Activity Product), but the latter refers to the *real* activities (different from the ideal condition at equilibrium).

In the reaction of precipitation of solids, the comparison between k_{sp} and IAP returns clues about the state of equilibrium (or not) of the solutions, and about the stability of the precipitated minerals.

When IAP>k_{sp} the solutions are oversaturated, and when ΔG>0 the mineral precipitates (and it is stable). Dolomite $CaMg(CO_3)_2$, compared to the other solids, showed the highest ΔG values (**Figure 8a,b**). A positive ΔG value means that the precipitation of the mineral occurs spontaneously.

However, as described further below, the equilibrium calculations revealed that dolomite and Ca-/Mg-carbonates in general may be inhibited in some conditions at relatively lower temperatures and lower pressures. The case of oversaturation of solutions with respect to dolomite is described further below.

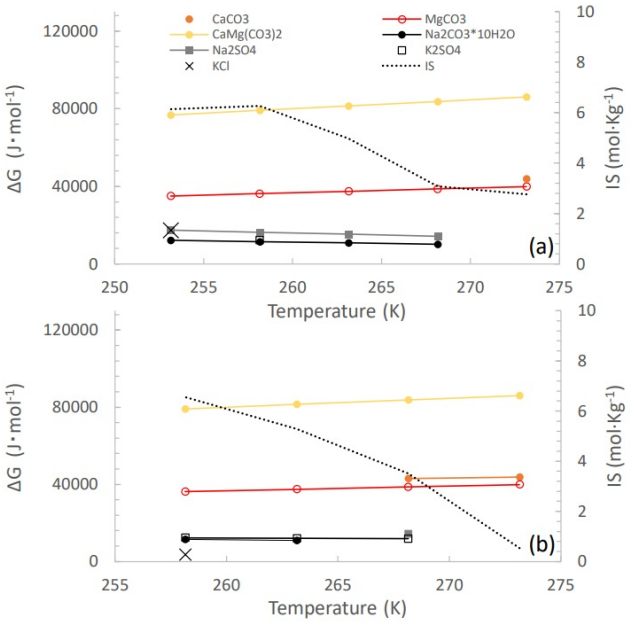

Figure 8. Standard of reactions of dissolution-precipitation equilibria calculated at each Δ temperature decrement for Kupalo (**a**) and Juling (**b**) at 1 bar of total pressure for carbonates, sulphates and chlorides. is given in J·mol^{-1} and for >0 solids precipitation is favored from aqueous solutions. In the same plots also IS values (the ionic strength of solutions; dotted curves) are given in right y-axis and expressed in mol·kg^{-1}.

5.3 Stability of Ca- and Mg-carbonates: The effect of temperature and pressure

We compared the above mentioned k_{sp} with IAP values of the ions involved in the reaction of precipitation.

Differences between k_{sp} and IAP are shown to understand what mineral is stable (the corresponding ions can precipitate from the solution) or unstable.

As shown in **Figure 9**, k_{sp} values in the dissociation-precipitation of $MgCO_3$ and $CaMg(CO_3)_2$ followed a power-law distribution and, in most cases, k_{sp} coincided with IAP values: that is, the solutions are saturated with respect to the minerals.

In that condition of saturation, by definition, the aqueous solution contains the maximum concentration of dissolved solute, compatible with its solubility limit, and therefore it is no longer possible to dissolve other so-

lutes without minerals precipitating. When the aqueous solutions are oversaturated with respect to the mineral, then IAP>k_{sp}.

A curious result is achieved by comparing IAP and k_{sp} values for the precipitation of dolomite during the freezing. At Kupalo, IAP and k_{sp} values in the reaction involving the precipitation of dolomite showed some differences (**Figure 9a,b**) considering slight variations of pressure.

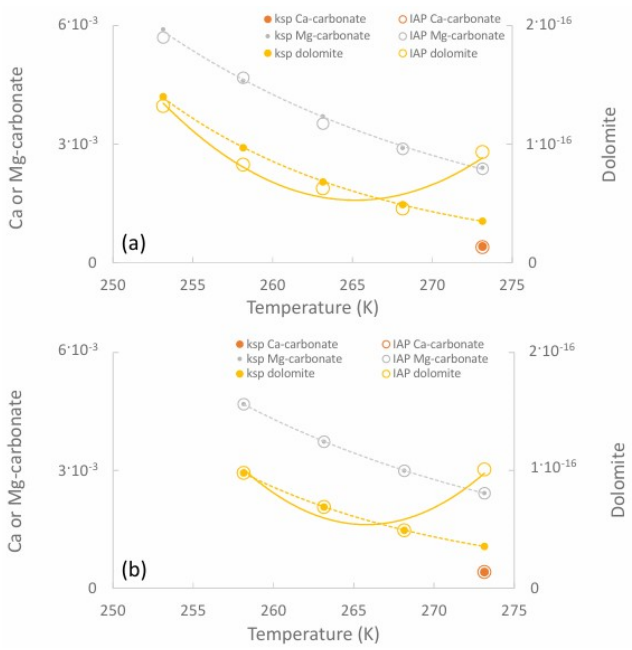

Figure 9. Comparison between equilibrium values and IAP for reactions involving the precipitation of Ca- and Mg-carbonates. $CaCO_3$ (orange symbols), $MgCO_3$ (grey symbols) and $CaMg(CO_3)_2$ (yellow symbols). The plot referred to Kupalo aqueous solutions at 1 bar (**a**) and 1.5 bar (**b**). At relatively higher pressure (**b**), the solutions were already oversaturated for dolomite at 273 K (IAP>k_{sp}) and saturated at T<270 K (IAP=k_{sp}).

Figure 9 shows that, at Kupalo, solutions were already oversaturated for dolomite at 273 K (IAP>k_{sp}) at 1 and 1.5 bar (**Figure 9a,b**). In other words, for dolomite, oversaturation is verified (at any pressure) for higher temperatures (T=273 K) at which the maximum stability of the mineral can be retrieved.

However, by freezing the solutions at different pressure values it is noted that, while, at higher pressure (**Figure 9b**) the solutions were saturated at T<270 K (IAP=k_{sp}, that means the solution are in equilibrium); instead, under shallower depth (1 bar; **Figure 9a**), the saturation is not verified. Possibly, under Kupalo, at a shallower depth, some processes, that directly involve other species, such as sodium, are more relevant. Moreover, **Figure 9a** returns the evidence that $MgCO_3$ (grey symbols in **Figure 9**) and $CaMg(CO_3)_2$(yellow symbols in **Figure 9**) precipitation can be inhibited at lower temperatures at 1 bar (where the solutions are not saturated at T<270 K, **Figure 9a**).

Under Juling (not shown here) no differences were found with pressure and, similarly to **Figure 9b**, for dolomite, IAP>k_{sp} at relatively higher temperature values.

6. Discussion

The initial aqueous solutions compositions under the selected craters differ for the availability of such species (e.g., higher chlorine and sodium amounts in Kupalo), in line with the high abundance of sodium carbonates found in Kupalo and not in Juling [15].

As input of our test, for Kupalo, we selected solutions that probably had a high amount of chlorine and sodium (**Table 1**), instead, Juling solutions were characterized by a low concentration of such iones.

For Juling crater's solutions, we can exclude that their sodium amount was about 1.4–1.8 (mol/kg) as in Occator [30] (**Table 1**) and as in Kupalo (this work). In fact, by setting the initial Na^+ concentration at value ≥ 0.8 moles/kg of water, Juling's aqueous solutions freezing models led to (unrealistic) precipitation of gypsum (at T=273 K) and other sulphates for further steps of FREZCHEM code, and no Ca- and Mg-carbonates could be formed (that are, instead, the predominant solids found in Juling deposits). For this reason, we reasonably inferred that Juling was characterized by sodium-depleted solutions (**Table 1**).

To exclude the possibility that Kupalo solutions were chlorine-depleted (as nearby Juling) we also carried out the simulations giving to Kupalo the initial chloride amount of 0.04 mol/kg, but, in that case, sodium-salts/carbonates never formed under Kupalo surface. The lack of sodium-salts and sodium-carbonates is not in line with results derived by Carrozzo et al. [15].

Concerning temperature, some authors reported that "the source of the surface bright salt deposits needs

to have T > 245 K for the Na- carbonate get in solution and T > 255 K for a significant concentration of melt to be present"[41]. In this work, we can suggest that temperature needs to be above 245 K to get aqueous solutions with dissolved Na+ and $CO_3{}^{2-}$; and, minute amount of unfrozen solution can exist at 255 K. In fact, for Kupalo, some solutions can exist, partially unfrozen, for T=255 K and the freezing process can continue for T<255K (**Figure 5**, **Figure 6a**).

About pressure, we do not exactly know if the bright spots have been generated from crustal brine pockets[47] or from deeper reservoirs[38]. However, we can speculate about surface processes of crustal heating that may occur at depths ranging from 3 hundred meters up to 1–10 kilometres (or more for greater impact events like Occator-forming).

6.1 Conditions for upwelling

The next considerations are important to explore the dynamics associated with the transport of brines in conduits and fractures induced by the low-pressure boiling and the crystallization of the possible reservoirs.

First, solids precipitation changes the aqueous solutions' density and viscosity. Kupalo and Juling solutions' densities (ρ_s), at the initial conditions, computed by FREZCHEM, were 1100 and 1025 kg·m^{-3} (the average densities were 1150 and 1130 kg·m^{-3}, respectively).

This implies that density values (which average is 1140 kg·m^{-3}) are lower than crust density[40] so that brines ascent (if triggered) could be the main mechanism to transport carbonate-rich material to the surface. To understand aqueous solutions' transport dynamics and speed (v) during possible upwelling, we could consider the velocity (v) as a function of solutions' densities (ρ_s), the viscosity (η_w), the Reynolds number (Re) and the radius of the conduit (R^*) as follows:

$$v = \frac{Re \cdot \eta_w}{\rho_s \cdot R^*} \tag{6}$$

where R^* is the radius of a possible cylindrical conduit, geometrically supposed to be smaller (R^* in a range of 10–100 meters) than the actual craters' radius (13 and 10 km for Kupalo and Juling, respectively[47]). This choice is compatible with the fact that vents are larger than the underlying feeding conduits[65] and because large conduits may not be structurally probable[66, 67]. Moreover, our radius range is in line with the size of active fractures on Europa moon[38, 67, 68].

During the freezing processes, η_w may be lower than the viscosity value given for the final stage of cryolavas ($\sim$102 Pa·s[38]) when brine has almost arrived in superficial fractures of the craters. We may assume that the viscosity (η_w) is ranged 1–10 Pa·s (which could correspond to the viscosity of the ice-solution mixture in which ice > solution). According to the flux regime in the conduit, we can impose that a laminar flux regime (100<Re<1000) is maintained in the conduit up to the surface. The end of laminar regime is fixed at Re =1000 (like in magmatic processes on Earth[69]).

Thus, under a laminar regime, brines may have a transport speed v, derived from Equation (6), in an order of 10^{-3}–10^{-4} m/s. A certain value of velocity is difficult to obtain since we don't have information about the real geometry of the conduit. Note that these are not the velocities achieved in the gas-jet plumes to vacuum which are out of the purpose of this study.

6.2 The effects of pressure and ionic strength on the gas solubility

The freezing processes could trigger the solidification of brines and the transport in subsurface conduits and fractures could be supported already in low crystallinity and low viscosity conditions. Then, when the solid fraction increases, another driving force may occur. For example, the emission of trapped gases may be another possible way of bringing carbonate-rich materials to the surface[42]. Transport speed values induced by gas expansions is beyond the purpose of our work, but it may be an additional element facilitating high density upwelling material[42].

In fact, during ascent, brines can be fragmented by the expansion of gas bubbles contained in clathrates that are not stable at low pressure[70] and, through decompression, they can irreversibly decompose with subsequent gas release[71]. The release of trapped gases and their constituent is dependent upon local conditions in terms of pressure and temperature. Moreover, the release of gas bubbles could play an important role in

the production of many of the characteristic ejecta morphologies, like those found in Kupalo, rather than Juling.

Here, we can try to show as the presence of little quantity of gas in brines, at decreasing pressure, can facilitate the ascent of material to the surface. To give an example, it can be noted that low amount of carbon dioxide ($CO_2$and $CO_{2,(g)}$) was probably present in the initial brines of Ceres[30] (**Table 1**). CO_2 solubility (in mol/kg of water) is inversely correlated to the concentration of aqueous solutions, that is our derived ionic strength (*IS*), and, as expected, it decreases in shallower pressure conditions. Then, during freezing, increasing *IS* values, led to decreasing CO_2 solubility in brines. The correlation between gaseous CO_2 solubility (mol/kg) and the ionic strength (IS, mol/kg), at fixed values of temperature and pressure, is reported in literature (the "Sechenov Law"[72]). We can try to adapt that correlation to our study according to the following equation:

$$log\frac{S_0}{S_{IS}} = k{\cdot}IS,\ [at\ T = 273K] \qquad (7)$$

with S_0 representing CO_2 solubility in pure water (S_0=0.0686 mol/kg at P=1 bar and S_0=0.3368 mol/kg at P=5 bar[73]), S_{IS} the CO_2 solubility in aqueous solution at different values of *IS* (x-axis in **Figure 10**), and k is the salt effect parameter determining the linear slope in the Equation (7).

For an easy visualization of the inverse relationship between CO_2 solubility and *IS* values of solutions, we plotted an inlet in **Figure 10**. For higher *IS* values of the aqueous solutions, the gas solubility in brines (S_{IS}) decreases.

In **Figure 10**, the black curve and the dotted one are derived from Duan and Sun[73] solubilities at 1 bar and 5 bar, respectively. To have a complete coverage of our case of liquid solutions moving at depths up to 10 km, we derived the correlation curve corresponding to 30 bar (blue line in **Figure 10**). CO_2 solubilities at 30 bar were computed starting from the data given from Duan et al.[74] and Li J. et al.[75].

The gas solubility is more affected by depth (already for IS>0.5 mol/kg, **Figure 10**); so that, at fixed *IS*, the solubility values are lower at low pressure (1 bar) and higher at high pressure (30 bar). Plausibly, therefore, the gas-driven transport of brines is more effective at the surface, especially for high-density ejecta. In other words, considering the high density of such sodium carbonates[42] the presence of dissolved (also low abundant) gas bubble in brines could facilitate the solids fragmentation and, if anhydrous phases are formed, these would more easily reach the surface.

To conclude, both mechanisms of low-pressure boiling of brines[30] and gas-driven transport may be considered as ways of bringing material to the surface.

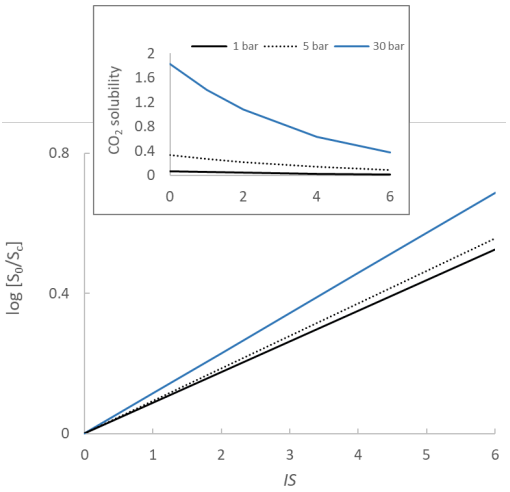

Figure 10. Plot showing the correlation between CO_2 solubility (mol/kg) and ionic strength (IS, expressed in mol/kg). The y-axis $log\frac{S_0}{S_c}$, is derived by Equation (7) in the text. For higher IS values of the aqueous solutions, the solubility of the gas is greater affected by depth. The correlation of Equation (7) is given for pressure values of 1 bar (black line) and 30 bar (blue line) which are our study case of solutions at corresponding depths from 300 m to 10 km. The dotted line is the correlation of Equation (7) using CO2 solubilities given by Duan and Sun[71] at 5 bar.

6.3 Salinity-temperature dependence

In our simulations, Kupalo solutions can be unfrozen at T=255 K and the freezing process can run for lower temperatures (**Figure 6**); on the contrary, for Juling, the freezing simulations stopped at T>255 K (**Figure 7**). Thus, it is possible to advance the existence of an inverse correlation between salinity of brines and the freezing temperature.

On Earth, the correlation between the salinity (expressed in g/kg) of a given solution and the freezing temperature (expressed in °C) is already given (Butler et al.[76] for sea ice brines, and, previously, Millero and Leung[77]).

In our system, we suggest that higher salinity (e.g., Kupalo-like solutions, with dissolved Na+ and Cl- higher than Juling-like solutions) may determine the existence of lower freezing temperatures suggesting, consequently, that Kupalo (or Kupalo-like solutions) may have a rate in the freezing process slower than nearby Juling.

Kupalo's brines, highly saline, could arrive to freeze to a lower temperature; and surface conditions could guarantee the formation and ejection of sodium-salts.

On the other hand, it is conceivable that minerals formed at high salinity conditions can be encapsulated in the pores of the ice. The correlation salinity-temperature for Ceres solutions was not found yet. In the future, the correlation between salinity of solutions, freezing temperature and porosity of grains may be validated by laboratory experiments carried out by using synthetic ice-salts-mixtures.

6.4 Precipitation of Na-salts from Na-enriched brines

Freezing simulations are in line with Thomas et al.[24] that demonstrated that hydrohalite may precipitate from brines at T<251.6 K from Na-enriched solutions. In addition, as suggested by experimental works of Thomas et al.[24], they can precipitate under a narrow set of conditions including a slow freezing process[32] that, as illustrated in the previous paragraph, could be typical processes occurring in Kupalo rather than in Juling.

We confirm that, at 1 bar of total pressure, hydrohalite can deposit from solutions in which both Na^+ and Cl^- ions are abundant (e.g., Na=1.8 and Cl=0.1 molal concentrations, Kupalo solutions). However, we were not able to determine the moles of hydrohalite precipitated below Kupalo by using the 1K and 5K model. A spectral feature due to possible hydrohalite was proposed[31] for Occator crater, whose aqueous solutions displayed high sodium content but variable amount in chlorine (from lower 0.01 to higher 0.08 moles/kg of water, **Table 1**). However, after its formation, in such conditions, hydrohalite can be transformed into anhydrous form (NaCl) that is IR inactive and not detectable by IR spectrometers like VIR.

However, very recently, Bramble and Hand[78] found that halite is a component of the bright surface areas at Ceres, and it may have been emplaced from subsurface liquid water that existed throughout time and space.

In this study, we found that sodium-salts, such as $NaHCO_3$ and $NaCl{\cdot}2H_2O$ are strongly pressure condition governed; their formation may occur at shallower layers at depth of few hundreds of meters below Kupalo.

In replicating our simulation for Na- and Cl-depleted solutions (Juling solutions), we observed that $NaCl{\cdot}2H_2O$ and $NaHCO_3$ did not precipitate, not even at 1 bar of total pressure.

$NaCl{\cdot}2H_2O$ and $NaHCO_3$ straight participate in the acid-base equilibria in aqueous solutions with CO_2[79] degassing promoting pH increasing[80] and influencing the precipitation rate of carbonates.

Finally, natrite (Na_2CO_3), found in Kupalo's surface layers[15, 28], did not directly precipitate from the solutions during the freezing simulations although, in sodium-rich environments (Kupalo), its hydrated form (natron, $Na_2CO_3{\cdot}10H_2O$) is favored.

Natrite could be directly formed from dehydration of natron ($Na_2CO_3{\cdot}10H_2O$) at total pressure ≥1 bar; or, alternatively, it can be derived at P=1 bar from nahcolite ($NaHCO_3$).

7. Conclusions

In this work, we investigated the freezing process of brines in Ceres' subsurface. Our simulations were performed using the FREZCHEM code[53, 62] assuming that potential Ceres' reservoir is characterized by presence of brines having the same physical properties as the ones summarized in Zolotov[30]. Our exercise was based on the selection of two geologically and close by young craters (Juling and Kupalo) hosting some of the most extensive carbonates rich areas and water ice[15, 28, 51], assuming an initial brines' temperature of 273 K (higher than the hosting-rocks). These simulations allowed us to speculate on whether different surface composition patterns - in terms of different carbonates contents as obtained with VIR spectral analysis - reflect different composition and differentiation of the initial aqueous solutions feeding the two regions under study.

The main results of our work can be envisioned as follows:

- The different minerals observed at Juling and Kupalo craters supports the scenario of initial subsurface aqueous solutions characterized by different chemical speciation. Another option is an evolution of the same initial composition. Such solutions may freeze at different pressure-temperature conditions.
- $MgCO_3$, $CaCO_3$ and $CaMg(CO_3)_2$ could have been the first solids to precipitate (before water ice formation). $MgCO_3$ and $CaMg(CO_3)_2$precipitation can be inhibited at lower temperature and pressure. Such solids are unstable at T<270 K at 1 bar for Na-enriched solutions.
- The formation of hydrated sodium carbonate (natron $Na_2CO_3 \cdot 10H_2O$) is highly favored in Na-enriched solution (e.g., Kupalo).
- Sodium bicarbonate, together with hydrohalite, can form under a narrow set of conditions (from bicarbonate alkaline aqueous solutions at P=1 bar); this does not contradict the scenario of a pressure-governed formation of $NaHCO_3$. Na^+ and HCO_3^- ions have been considered as possible components of brines[9, 30, 55], and some authors[24] suggested that $NaHCO_3$can form under a slow rate freezing process. Our results are consistent with this idea. In fact, we would suggest that at Kupalo, the potential solutions have frozen under rates lower than Juling, reaching to lower freezing temperature (**Figures 5** and **6a**).
  Moreover, the fact that some salts which generally form under fast freezing conditions, as NH_4Cl[24], have not been detected in Kupalo crater[15], seems to further support the hypothesis of a brines slow freezing, as also the results of our simulations do.

Some additional findings of this work help us to speculate on the freezing of specific solutions.

We investigated on the transport dynamics of the given brines in terms of viscosity and density in a potential cylindrical conduit. We suggest that, already in the subsurface, there could be the physical conditions to get brines to move toward shallower layers under sustained flow regime.

Low-pressure boiling of brines[30] and the gas-driven transport may be more decisive for bringing 1) high-density solids (as sodium carbonate particles), and 2) ice-dominated grains to the surface.

Gas-phase exsolution can be favourable in a high-salinity and high ionic strength condition, under shallower layers, facilitating the transport of carbonates-rich material to the surface.

We think that our approach might add some information about the explanation of the composition of Ceres' surface with respect to the retrieval from VIR. Based on visible and IR spectral absorption, VIR could have had a partial view of global mineralogical composition. That means that some minerals could be present on the surface but could not be "seen" by VIR because featureless in the spectral range of the instrument. This may be the case of some outputs of our freezing model: minerals could precipitate during the freezing of solutions, but the results of our model cannot be directly compared with VIR detection.

Some drawbacks of the current study may lead to future research complementing the results presented in this article.

We note that we have deliberately neglected to investigate the role of ammonia. During future investigations, the processes in which ammonium and sodium may be featured will be studied to a large extent. Indeed, revealing the details of the freezing processes within the Solar System will be an important step for future investigations aiming at the understanding of the planetary bodies' evolution.

Author contributions

Conceptualization, M.P.; methodology, M.P. and E.A.; software, M.P. and E.R.; investigation, all authors; data curation, all authors; writing-original draft preparation, M.P.; writing-review and editing, all authors; supervision, E.A. and M.C.D.S. All authors have read and agreed to the published version of the manuscript.

Funding

This research was funded by Agenzia Spaziale Italiana (ASI).

Institutional Review Board Statement

Not applicable.

Informed Consent Statement

Not applicable.

Data Availability Statement

Data deriving from the mission *Dawn* are available at repository PDS (Planetary Data System) at url: https://sbn.psi.edu/pds/resource/dawn/dwncvirL1.html and also https://sbib.psi.edu/data/PDS-Ceres/about.html. FREZCHEM code is available at url: https://www.dri.edu/frezchem.

Acknowledgments

This study was supported by the Directorate of Science and Innovation of ASI and by the Dawn VIR team at INAF-IAPS in Rome, Italy. The paper benefits from Dr. K. Holmberg's English edits, and of two anonymous reviewers' comments useful to improve the previous version.

Conflict of Interest

The authors declare that they have no conflict of interest.

References

[1] McCord, T.B., Combe, J.-P., Castillo-Rogez, J.C., et al., 2022. Ceres, a wet planet: The view after Dawn. Geochemistry. DOI: https://doi.org/10.1016/j.chemer.2021.125745

[2] De Sanctis, M.C., Coradini, A., Ammannito, E., et al., 2011. The VIR spectrometer. Space Sci. Rev. 163, 329–369.

[3] Li, J.-Y., McFadden, L.A., Parker, J.W., et al., 2006. Photometric Analysis of 1 Ceres and Surface Mapping from HST Observations. Icarus. 182(1), 143–160. DOI: https://doi.org/10.1016/j.icarus.2005.12.012

[4] Li, J.-Y., Schröder, S.E., Mottola, S., et al., 2019. Spectrophotometric Modeling and Mapping of Ceres. Icarus. 322, 144–167. DOI: https://doi.org/10.1016/j.icarus.2018.12.038

[5] Ciarniello, M., De Sanctis, M.C., Ammannito, E., et al., 2017. Spectrophotometric Properties of Dwarf Planet Ceres from the VIR Spectrometer on Board the Dawn Mission. Astronomy & Astrophysics. DOI: https://doi.org/0004-6361/201629490

[6] Ciarniello, M., De Sanctis, M.C., Raponi, A., et al., 2020. Ceres Observed at Low Phase Angles by VIR-Dawn. Astronomy & Astrophysics. DOI: https://doi.org/10.1051/0004-6361/201936492

[7] Lebofsky, L.A., Feierberg, M.A., Tokunaga, A.T., et al., 1981. The 1.7- to 4.2-μm Spectrum of Asteroid 1 Ceres: Evidence for Structural Water in Clay Minerals. Icarus. 48(3), 453–459. DOI: https://doi.org/10.1016/0019-1035(81)90055-5

[8] Rivkin, A.S., Volquardsen, E.L., Clark, B.E., 2006. The Surface Composition of Ceres: Discovery of Carbonates and Iron-rich Clays. Icarus. 185(2), 563–567. DOI: https://doi.org/10.1016/j.icarus.2006.08.022

[9] De Sanctis, M.C., Raponi, A., Ammannito, E., et al., 2016. Bright Carbonate Deposits as Evidence of Aqueous Alteration on (1) Ceres. Nature. 536, 54–57.

[10] King, T.V.V., Clark, R.N., Calvin, W.M., et al., 1992. Evidence for Ammonium-bearing Minerals on Ceres. Science. 255(5051), 1551–1553. DOI: https://doi.org/10.1126/science.255.5051.1551

[11] Milliken, R.E., Rivkin, A.S., 2009. Brucite and Carbonate Assemblages from Altered Olivine-rich Materials on Ceres. Nat. Geosci. 2(4), 258–261. DOI: https://doi.org/10.1038/ngeo478

[12] Rivkin, A.S., Li, J.-Y., Milliken, R.E., et al., 2012. The Surface Composition of Ceres. In: Redline S., Berger, N.A., (Eds.). The Dawn Mission to Minor Planets 4 Vesta and 1 Ceres. Springer: New York, NY, USA. pp. 95–116. DOI: https://doi.org/10.1007/S11214-010-9677-4

[13] Beck, P., Schmitt, B., Cloutis, E., et al., 2015. Low-temperature Reflectance Spectra of Brucite and the Primitive Surface of 1-Ceres? Icarus. 257, 471–476. DOI: https://doi.org/10.1016/j.icarus.2015.05.031

[14] Ammannito, E., DeSanctis, M.C., Ciarniello, M., et al., 2016. Distribution of Phyllosilicates on the Surface of Ceres. Science. 353. DOI: https://doi.org/10.1126/science.aaf4279

[15] Carrozzo, F.G., De Sanctis, M.C., Raponi, A., et al., 2018. Nature, Formation, and Distribution of carbonates on Ceres. Sci. Adv. 4(3). DOI: https://doi.org/10.1126/sciadv.1701645

[16] De Sanctis, M.C., Ammannito, E., Raponi, A., et al., 2015. Ammoniated Phyllosilicates with A Likely Outer Solar System Origin on (1) Ceres. Nature. 528, 241–244.

[17] Scully, J.E.C., Russell, C.T., Castillo-Rogez, J.C., et al., 2019. Introduction to the Special Issue: the Formation and Evolution of Ceres' Occator Crater. Icarus. 320, 1–6. DOI: https://doi.org/10.1016/j.icarus.2018.02.029

[18] Scully, J.E.C., Schenk, P.M., Castillo-Rogez, J.C., et al., 2020. The Varied Sources of Faculae-forming Brines in Ceres' Occator Crater, Emplacement via Hydrothermal Brine Effusion. Nat. Commun. 11, 3680.

[19] Raponi, A., De Sanctis, M.C., Carrozzo, F.G., et al., 2019. Mineralogy of Occator Crater on Ceres and Insight into Its Evolution from the Properties of Carbonates, Phyllosilicates, and Chlorides. Icarus. 320, 83–96. DOI: https://doi.org/10.1016/j.icarus.2018.02.001

[20] McSween, H.Y., Emery, J.P., Rivkin, A.S., et al., 2017. Carbonaceous Chondrites as Analogs for the Composition and Alteration of Ceres. Meteorit. Planet. Sci. 1–12. DOI: http://dx.doi.org/10.1111/maps.12947

[21] Postberg, F., Schmidt, J., Hillier, J., et al., 2011. A Salt-water Reservoir as the Source of a Compositionally Stratified Plume on Enceladus. Nature. 474, 620–622.

[22] Zambon, F., Raponi, A., Tosi, F., et al., 2017, Spectral Analysis of Ahuna Mons from Dawn Mission's Visible-infrared Spectrometer. Geophys. Res. Lett. 44, 97–104.

[23] Buczkowski, D.L., Sizemore, H.G., Bland, M.T., et al., 2018. Floor-fractured craters on Ceres and Implications for Interior Processes. Journal of Geophysical Research: Planets. 123, 3188–3204. DOI: https://doi.org/10.1029/2018JE005632

[24] Thomas, E.C., Vu, T.H., Hodyss, R., et al., 2019. Kinetic Effect on the Freezing of Ammonium-sodium-carbonate-chloride Brines and Implications for the Origin of Ceres' Bright Spots. Icarus. 320, 150–158. DOI: https://doi.org/10.1016/j.icarus.2017.12.038

[25] Sizemore, H.G., Schmidt, B.E., Buczkowski, D.A., et al., 2018. A Global Inventory of Ice-Related Morphological Features on Dwarf Planet Ceres: Implications for the Evolution and Current State of the Cryosphere. JGR Planets. DOI: https://doi.org/10.1029/2018JE005699

[26] Bowling, T.J., Ciesla, F.J., Marchi, S., et al., 2016. Impact Induced Heating of Occator Crater on Asteroid 1 Ceres. Proceedings of the 47th LPSC; The Woodlands, TX, USA; 21–25 March 2016. p. 2268.

[27] Bowling, T.J., Ciesla, F.J., Davison, T.M., et al., 2018. Post-impact Thermal Structure and Colling Timescales of Occator Crater on Asteroid 1 Ceres. Icarus. DOI: https://doi.org/10.1016/j.icarus.2018.08.028

[28] De Sanctis, M.C., Frigeri, A., Ammannito, E., et al., 2019. Ac-H-11 Sintana and Ac-H-12 Toharu Quadrangles: Assessing the large and Small Scale Heterogeneities of Ceres' Surface. Icarus. 318, 230–240. DOI: https://doi.org/10.1016/j.icarus.2017.08.014

[29] Ruiz, J., Jiménez-Díaz, A., Mansilla, F., et al., 2019. Evidence of Thrust Faulting and Widespread Contraction of Ceres. Nature astronomy. DOI: https://doi.org/10.1038/s41550-019-0803-2

[30] Zolotov, M.Y., 2017. Aqueous Origins of Bright Salt Deposits on Ceres. Icarus. 296, 289–304.

[31] De Sanctis, M.C., Ammannito, E., Raponi, A., et al., 2020. Fresh Emplacement of Hydrated Sodium Chloride on Ceres from Ascending Salty Fluids. Nature Astronomy. DOI: https://doi.org/10.1038/s41550-020-1138-8

[32] Vu, T.H., Hodyss, R., Johnson, P.V., et al., 2017. Preferential Formation of Sodium Salts from Frozen Sodium-ammonium-chloride-carbonate Brines—Implications for Ceres' Bright Spots. Planetary and Space Science. 141, 73–77.

[33] Fanale, F.P., Salvail, J.R., 1989. The Water Regime of Asteroid 1 Ceres. Icarus. 82, 97–110.

[34] Hayne, P.O., Aharonson, O., 2015. Thermal Stability of Ice on Ceres with Rough Topography. J. Geophys. Res. Planets. 120, 1567–1584. DOI: https://doi.org/10.1002/2015JE004887

[35] Formisano, M., De Sanctis, M.C., Magni, G., et al., 2016. Ceres Water Regime: Surface Temperature, Water Sublimation and Transient Exo(atmo)sphere. MNRAS. 455, 1892–1904. DOI: https://doi.org/10.1093/mnras/stv2344

[36] Bu, C., Rodriguez Lopez, G., Dukes, C.A., et al., 2019. Stability of Hydrated Carbonates on Ceres. Icarus. DOI: https://doi.org/10.1016/j.icarus.2017.12.036

[37] Zolotov, M.Y., 2020. The Composition and Structure of Ceres' Interior. Icarus. 335. DOI: https://doi.org/10.1016/j.icarus.2019.113404

[38] Quick, L.C., Buczkowski, D.L., Ruesch, O., et al., 2019. A Possible Brine Reservoir beneath Occator Crater: Thermal and Compositional Evolution and Formation of the Cerealia Dome and Vinalia Faculae. Icarus. 320, 119–135. DOI: https://doi.org/10.1016/j.icarus.2018.07.016

[39] Fu, R., Ermakov, E., Marchi, S., et al., 2017. The Interior Structure of Ceres as Revealed by Surface Topography. Earth Planet. Sci. Lett. 476, 153–164.

[40] Ermakov, A.I., Fu, R.R., Castillo-Rogez, J.C., et al., 2017. Constraints on Ceres' Internal Structure and Evolution from Its Shape and Gravity Measured by the Dawn Spacecraft. J. Geophys. Res. Planets. 122, 2267–2293.

[41] Hesse, M.A., Castillo-Rogez, J.C., 2019. Thermal Evo-

lution of the Impact-Induced Cryomagma Chamber Beneath Occator Crater on Ceres. Geophysical Research Letters. 46(3), 1213–1221. DOI: https://doi.org/10.1029/2018GL080327

[42] Ruesch, O., Quick, L.C., Landis, M.E., et al., 2019a. Bright Carbonate Surfaces on Ceres as Remnants of Salt-rich Water Fountains. Icarus. 320, 39–48. DOI: https://doi.org/10.1016/j.icarus.2018.01.022

[43] Ruesch, O., Genova, A., Neumann, W., et al., 2019b. Slurry Extrusion on Ceres from a Convective Mud-bearing Mantle. Nature Geoscience. 12(7), 1–5. DOI: https://doi.org/10.1038/s41561-019-0378-7

[44] Zolotov, M.Y., 2015. Physical Chemistry of Impact-generated Fluids and Bright Spots on Ceres. Meteorit. Planet. Sci. 50, 5384.

[45] Nathues, A., Platz, T., Thangjam, G., et al., 2017. Evolution of Occator Crater on (1) Ceres. Astronom. J. 153(3). DOI: https://doi.org/10.3847/1538-3881/153/3/112

[46] Ruesch, O., Nathues, A., Jaumann, R., et al., 2017. Faculae on Ceres: Possible Formation Mechanisms. Lunar Planet. Sci. 48, 2435.

[47] Stein, N.T., Ehlmann, B.L., Palomba, E., et al., 2019. The Formation and Evolution of Bright Spots on Ceres. Icarus. 320, 188–201. DOI: https://doi.org/10.1016/j.icarus.2017.10.014

[48] Hernandez, J., Nathues, A., Hiesinger, H., et al., 2022. Geology and Color of Kupalo Crater on Ceres. Planet. Space Sci. 220, 105538. DOI: https://doi.org/10.1016/j.pss.2022.105538

[49] Hernandez, J., Nathues, A., Hiesinger, H., et al., 2023. The Unique Floor of Juling Crater on Ceres. Planetary and Space Science. 239. DOI: https://doi.org/10.1016/j.pss.2023.105812

[50] Schmidt, B.E., Hughson, K.H.G., Chilton, H.T., et al., 2017. Geomorphological Evidence for Ground Ice on Dwarf Planet Ceres. Nature Geoscience. 10, 338–343.

[51] Raponi, A., De Sanctis, M.C., Frigeri, A., et al., 2018. Variations in the amount of water ice on Ceres' surface suggest a seasonal water cycle. Science Advances. 4, eaao3757. DOI: https://doi.org/10.1126/sciadv.aao3757

[52] Pitzer, K.S., 1995. Thermodynamics, 3rd ed. McGraw-Hill: New York, NY, USA. p. 626.

[53] Marion, G.M., Grant, S.A., 1994. FREZCHEM: A Chemical-thermodynamic Model for Aqueous Solutions at Subzero Temperatures. CRREL Special Report 94–18, Hanover, NH.

[54] Marion, G.M., Catling, D.C., Kargel, J.S., 2003. Modeling Aqueous Ferrous Iron Chemistry at Low Temperatures with Application to Mars. Geochim. Cosmochim. Acta. 67, 4251–4266.

[55] Castillo-Rogez, J.C., Neveu, M., McSween, H.Y., et al., 2018. Insights into Ceres's Evolution from Surface Composition. Meteoritics and Planetary Science. DOI: https://doi.org/10.1111/maps.13181

[56] De Angelis, S., Carli, C., Tosi, F., et al., 2019. NIR Reflectance Spectroscopy of Hydrated and Anhydrous Sodium Carbonates at Different Temperatures. Icarus. 317, 388–411. DOI: https://doi.org/10.1016/j.icarus.2018.08.012

[57] Saint-Pe, O., Combes, M., Rigaut, F., 1993. Ceres Surface Properties by High-Resolution Imaging from Earth. Icarus. 105, 271–281. DOI: https://doi.org/10.1006/icar.1993.1125

[58] Tosi, F., De Sanctis, M.C., Krohn, K., et al., 2016. Thermal Behavior of Bright Spots on Ceres. Proceedings of the 47th LPSC; The Woodlands, TX, USA; 21–25 March 2016. p. 1883.

[59] Capria, M.T., Tosi, F., De Sanctis, M.C., et al., 2014. Vesta Surface Thermal Properties Map. Geophysical Research Letters. 41(5), 1438–1443.

[60] Rognini, E., Capria, M.T., Tosi, F., et al., 2020. High Thermal Inertia Zones on Ceres from Dawn Data. Journal of Geophysical Research: Planets, 125, e2018JE005733. DOI: https://doi.org/10.1029/2018JE005733

[61] Palmer, E.M., Heggy, E., Letertre, T., et al., 2021. Exploring Ceres's Unusual Regolith Porosity and Its Implications for Volatile Retention. Planet. Sci. J. DOI: https://doi.org/10.3847/PSJ/ac0b3e

[62] Marion, G.M., Mironenko, M.V., Roberts, M.W., 2010. FREZCHEM: A Geochemical Model for Cold Aqueous Solutions. Computers & Geosciences. 36(1), 10–15. DOI: https://doi.org/10.1016/j.cageo.2009.06.004

[63] Langelier, W.F., Ludwig, H.F., 1942. Graphical Methods for Indicating the Mineral Character of Natural Waters. Journal American Water Works Association. 34(3), 335–352.

[64] Minissale, A., Magro, G., Martinelli, G., et al., 2000. Fluid Geochemical Transect in the Northern Apennines (Central-Northern Italy): Fluid Genesis and Migration and Tectonic Implications. Tectonophysics. 319(3), 199–222. DOI: https://doi.org/10.1016/S0040-1951(00)00031-7

[65] Wilson, L., Head, J.W., 2017. Generation, Ascent and Eruption of Magma on the Moon: New Insights into Source Depths, Magma Supply, Intrusions and Effusive/explosive Eruptions (Part 1: Theory). 283, 146–175. DOI: https://doi.org/10.1016/j.icarus.2015.12.039

[66] Miyamoto, H., Mitri, G., Showman, A.P., et al., 2005. Putative Ice Flows on Europa: Geometric Patterns and Relation to Topography Collectively Constrain Material Properties and Effusion Rates. Icarus. 177, 413–424.

[67] Quick, L.C., Marsh, B.D., 2016. Heat Transfer and

Cooling of Ascending Cryomagmas on Europa. J. Volcanol. Geotherm. Res. 319, 66–77.

[68] Fagents, S.A., 2003. Considerations for Effusive Cryovolcanism on Europa: The Post-Galileo Perspective. Journal of Geophysical Research. 108(E12), 5139. DOI: https://doi.org/10.1029/2003JE002128

[69] Lanzafame, G., Iezzi, G., Mancini, L., et al., 2017. Solidification and Turbulence (Non-laminar) during Magma Ascent: Insights from 2D and 3D Analyses of Bubbles and Minerals in an Etnean Dyke. Journal of Petrology. 58(8), 1511–1533. DOI: https://doi.org/10.1093/petrology/egx063

[70] Yasuda, K., Ohmura, R., 2008. Phase Equilibrium for Clathrate Hydrates Formed with Methane, Ethane, Propane or Carbon Dioxide at Temperatures below the Freezing Point of Water. J. Chem. Eng. Data. 53(9), 2182–2188. DOI: https://doi.org/10.1021/je800396v

[71] Kieffer, S.W., Lu, X., Bethke, C.M., et al., 2006. A Clathrate Reservoir Hypothesis for Enceladus' South Polar Plume. Science, 314, 5806. DOI: https://doi.org/10.1126/science.1133519

[72] Scharlin, P., (contributors: Cargill, R.W., et al.), 1996. Carbon Dioxide in Water and Aqueous Electrolyte Solutions. Oxford University Press, UK. Solubility data series. Volume 62, 383 p.

[73] Duan, Z., Sun, R., 2003. An Improved Model Calculating CO_2 Solubility in Pure Water and Aqueous NaCl Solutions from 273 to 533 K and from 0 to 2000. Chemical Geology. 193, 257–271. DOI: https://doi.org/10.1016/S0009-2541(02)00263-2

[74] Duan, Z., Sun, R., Zhu, C., et al., 2006. An Improved Model for the Calculation of CO2 Solubility in Aqueous Solutions Containing Na^+, K^+, Ca^{2+}, Mg^{2+}, Cl^-, and $SO_4{}^{2-}$. Marine Chemistry. 98, 131–139.

[75] Li, J., Ahmed, R., Li, X., 2018. Thermodynamic Modeling of CO_2-N_2-O_2-Brine-Carbonates in Conditions from Surface to High Temperature and Pressure. Energies. 11, 2627. DOI: https://doi.org/10.3390/en11102627

[76] Butler, B.M., Papadimitriou, S., Santoro, A., et al., 2016. Mirabilite Solubility in Equilibrium Sea Ice Brines. Geochim. Cosmochim. Acta. 182, 40–54.

[77] Millero, F.J., Leung, W.H., 1976. The Thermodynamics of Seawater at One Atmosphere. Am. J. Sci. 276, 1035–1077. DOI: https://doi.org/10.2475/ajs.276.9.1035

[78] Bramble, M.S., Hand, K.P., 2022. Spectral Evidence for Irradiated Sodium Chloride on the Surface of 1 Ceres. Geophysical Research Letters. 49, e2021GL096973. DOI: https://doi.org/10.1029/2021GL096973

[79] Anabaraonye, B.U., Crawshaw, J.P., Trusler, J.P.M., 2019. Brine Chemistry Effects in Calcite Dissolution Kinetics at Reservoir Conditions. Chemical Geology. 509, 92–102. DOI: https://doi.org/10.1016/j.chemgeo.2019.01.014

[80] Li, X., Peng, C., Crawshaw, J.P., et al., 2018. The pH of CO_2-saturated Aqueous NaCl and $NaHCO_3$ Solutions at Temperatures between 308 K and 373 K at Pressures up to 15 MPa. Fluid Phase Equilibria. 458, 253–263.